Analytic Theory of Tsunami Wave Scattering in the Open Ocean with Application to the North Pacific

H.O. Mofjeld, V.V. Titov, F.I. González, and J.C. Newman

Pacific Marine Environmental Laboratory
7600 Sand Point Way NE
Seattle, WA 98115

January 2000

NOTICE

Mention of a commercial company or product does not constitute an endorsement by NOAA/OAR. Use of information from this publication concerning proprietary products or the tests of such products for publicity or advertising purposes is not authorized.

Contents

List of Figures

List of Tables

Analytic Theory of Tsunami Wave Scattering in the Open Ocean with Application to the North Pacific

H.O. Mofjeld, V.V. Titov, F.I. González, and J.C. Newman

Abstract. A theory is developed to better understand the interaction of tsunami waves with small-scale, submarine topography in the open North Pacific Ocean. The tsunamis are assumed to be linear, long gravity waves at single frequencies. The topography is given simple forms from which explicit formulas can be derived for transmitted, reflected, and scattered waves. This topography includes linear features (escarpments and ridges) and circular seamounts. The theory shows that the most important factor determining the intensity of scattering and reflection is the depth of a feature compared with the depth of the surrounding region. A useful measure of this depth effect is the scattering index $S = 1 - T_{min}$, derived from the theory of lineal ridge scattering. Here $T_{min} = 2\epsilon/(1 + \epsilon^2)$, where $\epsilon \equiv \sqrt{H_1/H_0}$. For a regional depth of $H_0 = 5500$ m, features with depth shallower than $H_1 = 1500$ m interact significantly with tsunamis and those shallower than 400 m can have a major effect on these waves. The horizontal extent of a feature, compared with the wavelength, and the angle of incidence also affect the amount of scattering and reflection. Based on these criteria, the Emperor Seamount Chain, the Hawaiian Ridges, the Mid-Pacific Mountains, the Aleutian/Komandorskiye and Kuril Island Arcs, and the Shatsky and Hess Rises scatter and reflect transoceanic tsunamis. This interaction also increases the duration of these tsunamis. Simulating these processes with numerical models requires sufficiently accurate topography and high enough spatial resolution.

1. Introduction

The NOAA/PMEL Tsunami Research Program is carrying out a project to improve the U.S. Tsunami Warning System and the capability of the Pacific Disaster Center (González *et al.*, 1999). The project includes both modeling and observational components. The modeling component will lead to a database of simulated Pacific-wide tsunamis. Using the database, simulated tsunamis can be tuned quickly to earthquake information and to open-ocean tsunami observations. The tuned model tsunamis will then provide forecasts of tsunami wave heights for coastal communities in Alaska, Hawaii, California, Washington, Oregon, and the Pacific Insular States. Presently, the source regions for the model tsunamis are limited to the Alaska/Aleutian Subduction Zone (AASZ). However, plans are in place to expand the source region to include the entire Pacific Rim. The open-ocean observations will be reported in real time by an array of Deep-ocean Assessment and Reporting of Tsunamis (DART) buoys in the North Pacific Ocean and a station near the Equator.

   A goal of this work is to provide this guidance to the NOAA Tsunami Warning Centers and the Pacific Disaster Center within an hour following a tsunamigenic earthquake in the Pacific Region. Having a rapid procedure is required in order to give emergency managers as long a lead time as possible before the tsunamis reach their regions of responsibility. It is also intended that this guidance will lead to a reduction in the number of false tsunami warnings and unnecessary evacuations. Details of the NOAA/PMEL Tsunami Program, the Method Of Splitting Tsunami (MOST) numerical model database (Titov *et al.*, 1999), and the DART buoy system

are given at the Tsunami Program's Web site (URL: `http://www.pmel.`
`noaa.gov/tsunami/`).

While doing MOST model simulations of tsunamis in the North Pacific,
a number of issues arose concerning the effects of fine-scale topography on
Pacific-wide tsunamis. A study was then carried out to investigate these
issues. There were four main goals for the study: (a) understand how fine-
scale topography affects tsunami wave propagation, (b) develop simple cri-
teria for identifying topographic features that reflect and scatter significant
tsunami energy, (c) interpret the tsunami wave-height patterns seen in the
MOST model simulations, and (d) determine how smoothing the topogra-
phy affects the model tsunamis. The preliminary results of the study were
presented at the IUGG 99 Tsunami Symposium by Mofjeld *et al.* (1999b).

In this technical memorandum, we present the analytic theory that was
developed to address the first two goals. It is an application of linear, long-
wave theory to the scattering of tsunami waves off idealized forms of topogra-
phy. The analytic theory is meant to provide tools to use when interpreting
the results of the MOST numerical model. No claim is made that the bulk of
the theory is either original or comprehensive. Indeed, the theory is meant
to be as limited and simple as possible. Even so, it is still extensive enough
to unduly burden a publication in the peer-reviewed literature. This techni-
cal memorandum was therefore written to describe the theory in sufficient
detail to act as a reference for publications describing the effects of realistic
topography on Pacific-wide tsunamis. For a general overview and bibliogra-
phy on tsunami prediction research, please see the recent review by Mofjeld
et al. (1999a). What is new in the theory is the concept of minimum trans-
missivity and a scattering index S. This index turns out to be very useful
in identifying major scattering features in the open ocean.

Although tsunami scattering is weak over low topographic features (Car-
rier, 1971), recent model studies show that a number of features in the North
Pacific do scatter substantial tsunami energy (Mofjeld *et al.*, 1999b). Much
of the finer-scale topography in the North Pacific consists of lineal features
such as escarpments, ridges, and trenches. Many of these have cross-feature
scales of tens to hundreds of kilometers but extend in length over thousands
of kilometers. These are the cross-feature scales that are most relevant to
tsunami wave scattering in the open ocean. The large extent of these features
means that any tsunami propagating across the North Pacific will encounter
a number of these features. There are also extensive fields of seamounts in
the region.

The technical memorandum is organized as follows. After this introduc-
tion are four sections deriving the analytic theory: basic formulation, es-
carpments, ridges and trenches, and circular seamounts. These provide the
essential formulas and interpretative tools for the discussion section, which
identifies the major scattering features in the North Pacific. Concluding the
technical memorandum is a summary of results. Readers may find it efficient
to look over the next section on the basic formulation of the theory and then
go directly to the Discussion and Conclusions (Sections 6–7), referring back
to the detailed theoretical sections as needed.

2. Basic Formulation

The analytic theory is based on long waves interacting with idealized topography in the open ocean. In the theory, we neglect the relatively small effects of non-linear processes, dispersion and friction in the open ocean, as well as the Coriolis effect. It turns out that the amount of scattering often depends on a feature's spatial extent relative to the tsunami wavelength or, more precisely, the phase shift across the feature. To include this dependence in the theory, each tsunami is assumed to occur at a given frequency. Hence, the theory may be thought of as a frequency analysis of tsunami wave scattering. The focus of the theory is on scattering at locations that are well away from the source and impact regions. The incident tsunami waves can then be approximated by plane waves. While the long wave equations and formulas for plane waves are readily available in many references and textbooks, it is convenient to repeat them here in order to define the notation.

The long waves satisfy linearized equations of motion in the surface elevation η and the wave transport $\mathbf{Q} = H\,\mathbf{u}$, which is the product of the water depth H and the horizontal water velocity $\mathbf{u} = (u_x, u_y)$

$$\frac{\partial\,\mathbf{Q}}{\partial\,t} = -\,g\,H\,\bigtriangledown\eta \tag{1}$$

$$\frac{\partial\,\eta}{\partial\,t} = -\,\bigtriangledown\cdot\mathbf{Q} \tag{2}$$

where t is time and g is the acceleration of gravity.

For constant depth H, these equations have plane wave solutions of the form

$$\begin{bmatrix}\eta \\ \mathbf{Q}\end{bmatrix} = A\begin{bmatrix}1 \\ c\,\hat{\mathbf{k}}\end{bmatrix}e^{\,i\,[\mathbf{k}\cdot\mathbf{x}\,-\,\omega t]} \tag{3}$$

where A is the complex amplitude, $c = \sqrt{gH}$ is the long wave speed, $\hat{\mathbf{k}}$ is the unit vector pointing in the same direction as the wavenumber $\mathbf{k} = (k_x, k_y)$, $\mathbf{x} = (x, y)$ is the horizontal distance vector, and ω is the angular frequency.

Defining the incident angle ϕ relative to the x-axis, the unit direction vector $\hat{\mathbf{k}}$ can be written

$$\hat{\mathbf{k}} = (\cos\phi,\ \sin\phi)\,. \tag{4}$$

In the following sections, analogous notation will be defined for reflected waves scattered off lineal topography (rectangular coordinate system) and for waves scattered off seamounts (cylindrical coordinate system).

A useful concept to apply to wave scattering problems is the conservation of energy flux. This principle requires that without dissipation, a steady flux into a region must be balanced by an equal flux out of the region. To apply the principle to scattering and reflection of tsunami waves inside a region, it is convenient to write the fluxes as integrals over the bounding surface of the flux density. For a two-dimensional plane wave (3) the flux density,

integrated over depth, is defined as the energy propagating per unit time and per unit width

$$\mathbf{F} \;=\; \rho\, g\, c\, \hat{\mathbf{k}}\, \frac{|A|^2}{2}\;.\tag{5}$$

It is a vector in the direction of the wavenumber $\mathbf{k}$ and is proportional to the water density ρ, the acceleration of gravity g, the long wave speed c, and the square of the wave amplitude's magnitude $|A|$. Since this form (5) has been integrated over depth, each integral around the bounding surface becomes a line integral of the normal component of the energy flux density.

For lineal topographic features (such as escarpments, ridges, and trenches), rectangular regions provide simple forms for the flux components at the bounding surfaces if two sides are oriented parallel to the features. When an incident wave is planar, the transmitted and reflected waves are also planar. Conservation of energy flux then reduces to a simple balance between flux densities. In vector form,

$$\mathbf{F}_I + \mathbf{F}_R = \mathbf{F}_T\tag{6}$$

where the subscripts refer to incident (I), reflected (R), and transmitted (T) waves.

In the case of scattering off an isolated circular features, a circular region centered on the seamount provides simple formulas for the fluxes. For instance, Lamb (1932) uses the flux out of such a region to estimate the amplitudes of scattered waves resulting from the interaction of plane waves with circular islands.

2.1   Lineal Step Topography: Normal Incidence

The theory uses stepwise topography to approximate the real topography. These steps consist of constant-depth segments, separated by vertical transitions in depth. For lineal topography (escarpments, ridges and trenches), we orient the coordinate system so that the topography varies only in the x-direction. In this subsection, we concentrate mainly on normal incidence $(\phi = 0°)$. Then within the j-th segment $(x_j, < x < x_j + \delta x_j)$, the water depth H_j is constant and the phase velocity c_j and incident x-wavenumber k_j component (dropping the subscript x) are

$$c_j = \sqrt{gH_j} \quad \text{and} \quad k_j = \frac{\omega}{c_j}\tag{7}$$

For normal incidence the incident wave has the form

$$\begin{bmatrix} \eta_j \\ Q_j \end{bmatrix} = A_j \begin{bmatrix} 1 \\ c_j \end{bmatrix} e^{\,i\,[\theta_j(x)-\omega t]}\tag{8}$$

where the cumulative phase $\theta_j(x)$ is given by

$$\theta_j(x) = \theta_0 + k_j(x - x_j) + \sum_{j'=1}^{j} k_{j'-1}(x_{j'} - x_{j'-1})\;.\tag{9}$$

Here, the last term is the sum of the individual contributions to the phase that are made as the wave propagates across each topographic step leading to the j-th step.

For the reflected wave, we use ξ_j to denote the surface elevation, R_j the water transport, and B_j the complex amplitude. Since this wave is propagating in the opposite direction (in the negative x-direction) from the incident wave, we reverse the signs of the transport ($c_j \rightarrow -c_j$) and the phase ($\theta_j \rightarrow -\theta_j$) in (8)

$$\begin{bmatrix} \xi_j \\ R_j \end{bmatrix} = B_j \begin{bmatrix} 1 \\ -c_j \end{bmatrix} e^{i\,[-\theta_j(x)-\omega t]} \tag{10}$$

The location of the origin $x = 0$ and the phases of the complex amplitudes $A(0)$ and $B(0)$ at $x = 0$ are chosen to be the most convenient for the particular topographic feature or the method of solution.

Linear wave theory requires that two quantities be continuous at an abrupt change in water depth: the total surface elevation and the component of the total water transport that is perpendicular to the transition in depth. In the case of normal incidence on lineal topography varying only in the x-direction, these conditions for the depth transition at $x = x_j$ are

$$\eta_{j-1} + \xi_{j-1} = \eta_j + \xi_j \tag{11}$$

$$Q_{j-1} + R_{j-1} = Q_j + R_j \tag{12}$$

Substituting for the normal transports in terms of the surface elevations and using (7),

$$c_{j-1}\,[\eta_{j-1} - \xi_{j-1}] = c_j\,[\eta_j - \xi_j] \tag{13}$$

or

$$\eta_{j-1} - \xi_{j-1} = \epsilon_j\,[\eta_j - \xi_j] \tag{14}$$

where

$$\epsilon_j \equiv \left[\frac{H_j}{H_{j-1}} \right]^{\frac{1}{2}}. \tag{15}$$

When the matching conditions are applied to all the transitions in the region, the resulting matching equations lead to the formulas describing the wave scattering by the full topographic feature. When the subscript j is dropped, the depth parameter ϵ corresponds to the minimum depth of a feature relative to the depth of the nearby region over which the incident waves propagate to the feature. As we will see throughout the rest of this memorandum, ϵ plays a fundamental role in the scattering theory.

2.2   Continously Varying Topography

The theory for continuously varying topography is based on the matching equations (11–14) in which the segment widths are allowed to go to zero

$(\delta x_j \to 0)$. The derivation given below is for normal incidence. It is convenient to use the wave speeds c_j in the analysis. Solving (11–14) for η_j and ξ_j leads to symmetric equations for the two waves

$$\eta_j - \eta_{j-1} = -\frac{\delta c_j}{2c_j} \left[\eta_{j-1} - \xi_{j-1}\right] \tag{16}$$

$$\xi_j - \xi_{j-1} = -\frac{\delta c_j}{2c_j} \left[\xi_{j-1} - \eta_{j-1}\right] \tag{17}$$

where $\delta c_j \equiv c_j - c_{j-1}$.

Writing the surface elevations η_{j-1} and ξ_{j-1}, evaluated at the matching location $x = x_j$, as

$$\eta_{j-1} = A_{j-1}\,e^{i\theta_j} \qquad \text{and} \qquad \xi_{j-1} = B_{j-1}\,e^{-i\theta_j} \tag{18}$$

and using the phase relation

$$\theta_j = \theta_{j-1} + k_{j-1}\delta x_j \tag{19}$$

where

$$k_{j-1} = \frac{\omega}{c_{j-1}} \qquad \text{and} \qquad \delta x_j = x_j - x_{j-1} \tag{20}$$

leads to difference equations for the wave amplitudes

$$A_j - A_{j-1} = -\frac{\delta c_j}{2c_j} \left[A_{j-1} - B_{j-1}\,e^{-2i\theta_j}\right] \tag{21}$$

$$B_j - B_{j-1} = -\frac{\delta c_j}{2c_j} \left[B_{j-1} - A_{j-1}\,e^{2i\theta_j}\right]\,. \tag{22}$$

Dividing (21–22) by δx_j and taking the limit $\delta x_j \to 0$ leads in turn to the differential equations in the amplitudes $A(x)$ and $B(x)$

$$\frac{dA}{dx} = -\beta A + \beta B\,e^{-2i\theta} \qquad \text{and} \qquad \frac{dB}{dx} = -\beta B + \beta A\,e^{2i\theta} \tag{23}$$

where

$$\beta \equiv \frac{1}{2c}\frac{dc}{dx} \tag{24}$$

and the phase $\theta(x)$ is given by the integral of wavenumber over x

$$\theta(x) = \int_0^x k(x')\,dx'\,. \tag{25}$$

The boundary conditions on the amplitude A of the incident wave is that it is equal to a known value A_0 at a location $x = 0$ that is well before the wave reaches the topography of interest

$$A = A_0 \qquad \text{at} \quad x = 0\,. \tag{26}$$

The condition on the amplitude B is that the back-scattered wave has no source on the far side of the topographic feature. Hence,

$$B \to 0 \qquad \text{as} \quad x \to \infty . \tag{27}$$

Equations (23) can be simplified by using modified amplitudes A' and B' that incorporate Green's $\frac{1}{4}$th–law

$$A = \left[\frac{H}{H_0}\right]^{-\frac{1}{4}} A' \qquad \text{and} \qquad B = \left[\frac{H}{H_0}\right]^{-\frac{1}{4}} B' . \tag{28}$$

The differential equations (23) then take the form

$$\frac{dA'}{dx} = \beta B' e^{-2i\theta} \qquad \text{and} \qquad \frac{dB'}{dx} = \beta A' e^{2i\theta} \tag{29}$$

which can be integrated to give

$$A' = A_0' + \int_0^x \beta(x') B' e^{-2i\theta'} dx' \tag{30}$$

$$B' = B_0' + \int_0^x \beta(x') A' e^{2i\theta'} dx' \tag{31}$$

where

$$\theta' = \int_0^{x'} k(x'') \, dx'' .$$

The phase terms in the integrands of (30–31) contain factors of two in the exponents because the total phase shift is the sum of two terms: the phase shift θ' due to forward propagation of the incident wave to a scattering site and another shift of θ' for the propagation of the scattered wave returning from that site.

In this memorandum, the scattering by continuously varying topography is limited to low relief. In this case, the topographic scattering is weak enough that the incident amplitude A_0 can be substituted into the equation (31) for A'. For an isolated topographic feature that is limited in extent ($\beta = 0$ for $|x| >$ some x_1),

$$B' \doteq B_0' + \int_0^x \beta(x') A_0' e^{2i\theta'} dx' \tag{32}$$

or

$$B' \doteq B_0' + A_0' \int_0^x \beta(x') e^{2i\theta'} dx' . \tag{33}$$

Using the boundary condition (27) on B leads to a first approximation for amplitude of the scattered wave

$$0 \doteq B_0' + A_0' \int_0^\infty \beta(x') e^{2i\theta'} dx' . \tag{34}$$

Changing the origin ($x = 0$) so that it is centered on the topographic feature and extending the lower limit ($x \to -\infty$) of the integer in (34), the amplitude B_0 of the scattered wave is given approximately by

$$B_0 \doteq -A_0 \int_{-\infty}^{\infty} \beta(x') \, e^{2i\theta'} \, dx' \, . \tag{35}$$

At the same order of approximation the incident wave is unaffected by the small-slope topography (more precisely, topography where $\beta/k_0 \ll 1$), other than the Green's law variations in amplitude and cumulative shifts in phase away from $k_0 x$. This is the WKBJ approximation for the interaction of a tsunami wave with topography

$$\eta(x) \doteq A_0 \left[\frac{H}{H_0} \right]^{-\frac{1}{4}} e^{i\theta} \quad , \quad \theta = \theta_0 + \int_{x_0}^{x} k(x') \, dx' \, . \tag{36}$$

A first correction to the amplitude of the transmitted wave, due to scattering, can be made using the conservation of energy flux (5–6).

In the following sections, the theory for continuously varying topography will be applied to two cases. The first case is an escarpment having an error function profile in depth, and the second is a ridge having a Gaussian profile. These cases provide a way of identifying those processes predicted with step topography that are likely to occur when tsunami waves encounter more realistic topography. They also identify three frequency regimes: where the step-topography theory applies, a continuous theory is needed, and the WKBJ approximation adequately describes the behavior of the waves.

3.   Lineal Escarpments

This section on lineal (straight) escarpments focuses on scattering and reflection by single transitions in depth. The simplest case is a step transition when the tsunami wave approaches at normal incidence ($\phi = 0°$). For this case, the behavior of the wave is dependent only on the depth parameter ϵ and is independent of the wave frequency ω. At other incident angles ϕ, the behavior is similar to the case of normal incidence except when the tsunami waves approach the escarpment from the shallow side. Then, the waves can be perfectly reflected for $\phi > \phi_{crit}$, which depends on frequency ω. The last part of the section deals with a continuous depth transition in the form of an error function profile. The extension to non-normal incidence is straightforward. This section also provides essential background for the following one on scattering by ridges and trenches.

3.1   Vertical Step Escarpment: Normal Incidence

Letting H_0 be the depth on the side of a step escarpment (Figure 1) with the incident wave and letting H_1 be the depth on the other side, the matching equations (11 and 14) lead to the following relations between the wave
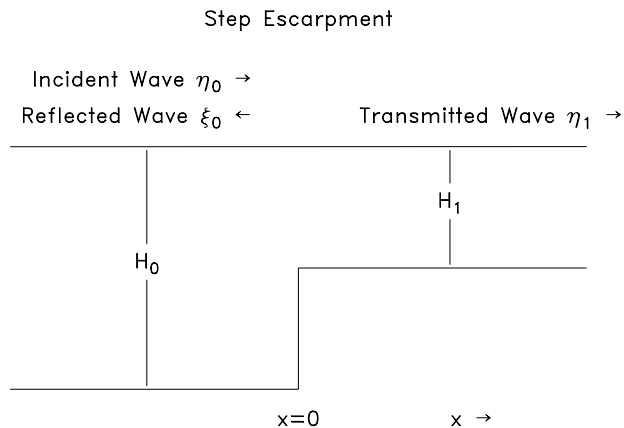
Step Escarpment

Incident Wave η_0 →

Reflected Wave ξ_0 ←   Transmitted Wave η_1 →

H_1

H_0

x=0   x →

Figure 1: Schematic diagram of a step escarpment having a vertical transition between two constant-depth regions H_0 and H_1. View is edge-on.

amplitudes

$$A_I + B_R = A_T \tag{37}$$

$$A_I - B_R = \epsilon A_T \tag{38}$$

where A_I is the amplitude of the incident wave, B_R is the amplitude of the reflected wave, A_T is the amplitude of the transmitted wave, and $x = 0$ at the escarpment. Here, the subscript has been dropped from the depth parameter $\epsilon \equiv \epsilon_1$.

Note that the matching conditions (37–38) do not change as the wave frequency ω is changed. Hence, the results for the step escarpment are independent of ω when the tsunami waves approach the escarpment with normal incidence.

Solving (37–38) for the amplitude ratios $R_T \equiv A_T/A_I$ and $R_R \equiv B_R/A_I$,

$$R_T = \frac{2}{1+\epsilon} \qquad \text{and} \qquad R_R = \frac{1-\epsilon}{1+\epsilon} \, . \tag{39}$$

Figure 2 shows how the amplitude ratios R_T and R_R vary with ϵ. When the incident wave approaches from the deep side of the escarpment ($\epsilon < 1$), the amplitude A_T is larger than A_I; and the amplitude B_R of the reflected wave is positive. As the depth parameter ϵ becomes smaller, the greater depth contrast across the escarpment causes $A_T \to 2 \times A_I$ and $B_R \to A_I$.

Conversely, there is negative reflection ($B_R < 0$) when the incident wave approaches from the shallow side ($\epsilon > 1$). In this case, increasing depth contrast leads to smaller $A_T \to 0$ and $B_R \to -1$. Hence, large depth contrasts ($|\epsilon| \gg 1$) produce strong wave reflection ($|R_R| \to 1$) regardless of whether the incident wave approaches the escarpment from the deep or the shallow side.

The transition (Figure 2) between the two asymptotic regimes passes through $\epsilon = 1$ where there is perfect transmission ($R_T = 1$) and no reflection
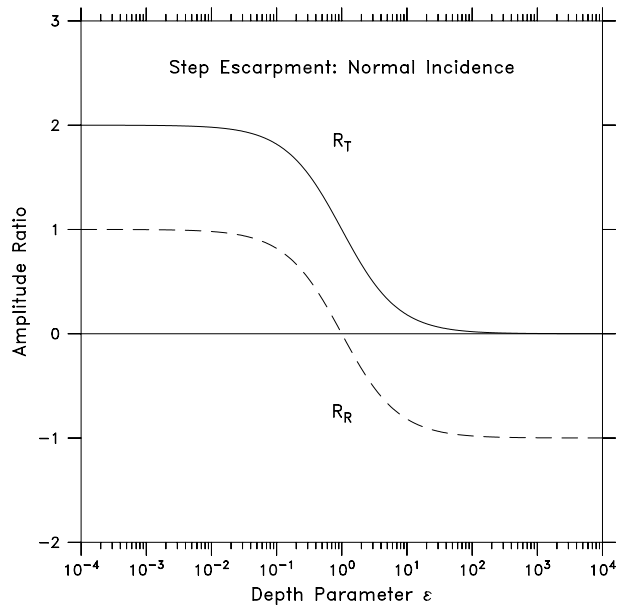
Figure 2: Amplitudes of reflected and transmitted tsunami waves resulting from the interaction of a normally incident wave ($\phi = 0°$) on a step escarpment, as a function of the depth parameter $\epsilon = \sqrt{H_1/H_0}$. The amplitudes are shown as ratios relative to the amplitude A_0 of the incident wave.

$(R_R = 0)$. The width of the transition can be measured by the end-values of the range $1.9 \geq T \geq 0.1$. Using this criterion, the transition scans $1/19 \leq \epsilon \leq 19$. The maximum rate of change of R_T and R_R occurs when $\epsilon = 1$

$$\max\left[\frac{dR_T}{d\epsilon}\right] = \max\left[\frac{dR_R}{d\epsilon}\right] = -2 \,. \tag{40}$$

Using (5), the transmitted energy flux F_T can then be written

$$F_T = \frac{4\epsilon}{(1+\epsilon)^2} \, F_I \qquad \text{and} \qquad F_R = -\frac{(1-\epsilon)^2}{(1+\epsilon)^2} \, F_I \,. \tag{41}$$

As Figure 3 shows, the energy flux F_T of the transmitted wave has a maximum value of unity (perfect transmission) at $\epsilon = 1$ and decreases toward zero energy transmission as the depth contrast increases. This includes the case in which the transmitted wave $A_T \to 2 \times A_I$ in which the escarpment shoals to a very shallow depth on the side opposite the incident wave. The energy flux F_T of the transmitted wave is zero at $\epsilon = 1$ and increases with the depth contrast in such a way that the total energy flux (6) is conserved.
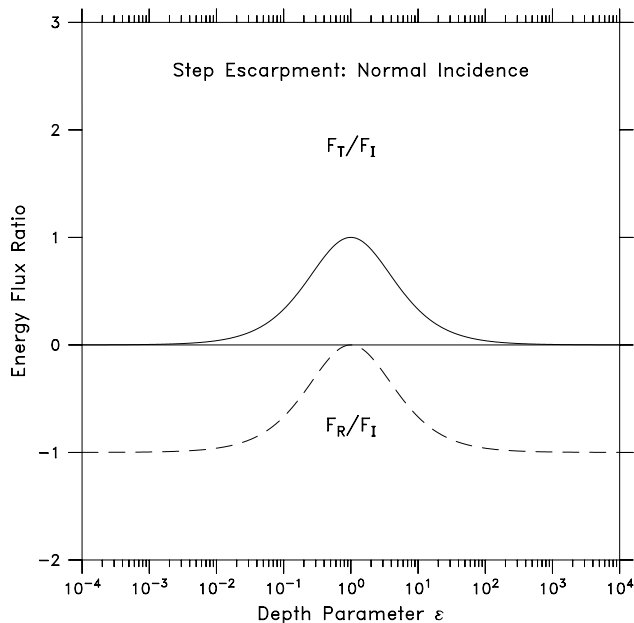
Figure 3: Energy flux components in the direction of wave propagation for the reflected F_R and transmitted F_T tsunami waves resulting from the interaction of a normally incident wave on a step escarpment, as a function of the depth parameter ϵ. The fluxes are shown as ratios relative to the flux F_I of the incident wave.

3.2   Vertical Escarpment: Non-Normal Incidence

When the incident wave (Figure 4) approaches a step escarpment from a non-normal angle ($\phi_0 \neq 0°$), the incident, reflected, and transmitted waves all satisfy the dispersion relation

$$k_{x,j} = k_j \cos \phi_j \quad \text{and} \quad k_{y,j} = k_j \sin \phi_j \qquad \text{where } k_j \equiv \frac{\omega}{c_j} . \qquad (42)$$

For the step escarpment, Snell's law of refraction (derived from the constancy of k_y across the y-independent topography $k_{y,1} = k_{y,0}$), determines the direction ϕ_1 of the transmitted wave in terms of the incident angle ϕ_0 and the depth parameter ϵ

$$\phi_1 = \arcsin(\epsilon \sin \phi_0) . \qquad (43)$$

As shown in Figure 4, refraction causes the transmitted wave to turn more normal ($\phi_1 < \phi_0$) when the incident wave approaches from the deep side of the escarpment ($\epsilon < 1$).

Conversely, it is less normal ($\phi_1 > \phi_0$) when the incident wave approaches from the shallow side ($\epsilon > 1$). Unlike normal incidence, it is possible for the incident wave to be perfectly reflected by the escarpment when the incident wave approaches from the shallow side of the escarpment. That is, there
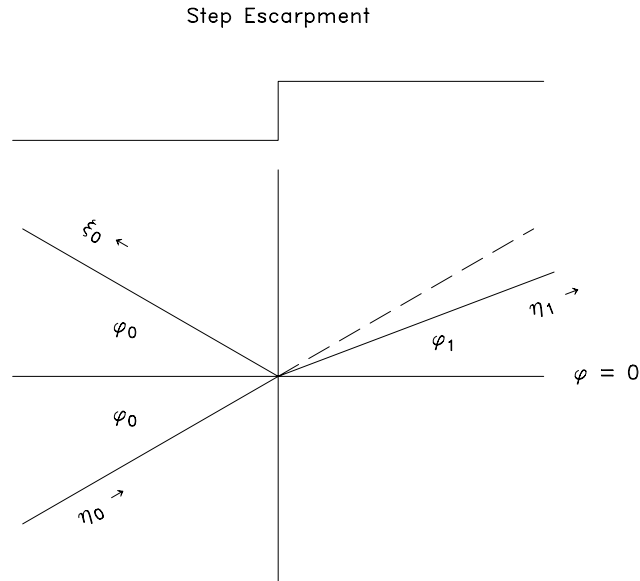
Step Escarpment

Figure 4: Schematic diagram showing the angles of incident (ϕ_0) and refracted (ϕ_1) waves as a tsunami wave propagates obliquely across a step escarpment. $\phi_1 < \phi_0$ indicates that the incident wave is approaching from the deep side of the escarpment.

is a critical incident angle $[\phi_0]_{crit}$ beyond which the transmitted wave is evanscent ($k_{x,1}$ imaginary). A formula for this angle can be derived from the dispersion relation

$$(k_{x,j})^2 = \frac{\omega^2}{c_j^2} - (k_{y,j})^2 \tag{44}$$

by noting that $k_{y,1} = k_{y,0}$ and setting $k_{x,1} = 0$

$$0 = \frac{\omega^2}{c_1^2} - k_{y,0}^2 . \tag{45}$$

Using (42) leads to

$$[\phi_0]_{crit} = \arcsin\left(\epsilon^{-1}\right) \quad , \qquad \epsilon \geq 1 . \tag{46}$$

Figure 5 shows that the critical angle $[\phi_0]_{crit}$ decreases rapidly as ϵ increases past $\epsilon = 1$. Since tsunami waves are not likely to have exactly normal incidence on an escarpment, the theory suggests that there is a strong tendency for tsunami waves to be reflected at a sharp transition from very shallow water to the deep ocean. This tendency is much less pronounced for oceanic escarpments since rarely is $\epsilon > 1.1$ for escarpments in the North Pacific, except for the Mendocino Escarpment.

Formulas for the transmissivity and reflectivity can be derived for non-normal incidence using modified versions of the matching conditions (37–38). While the matching condition for surface elevation remains the same,
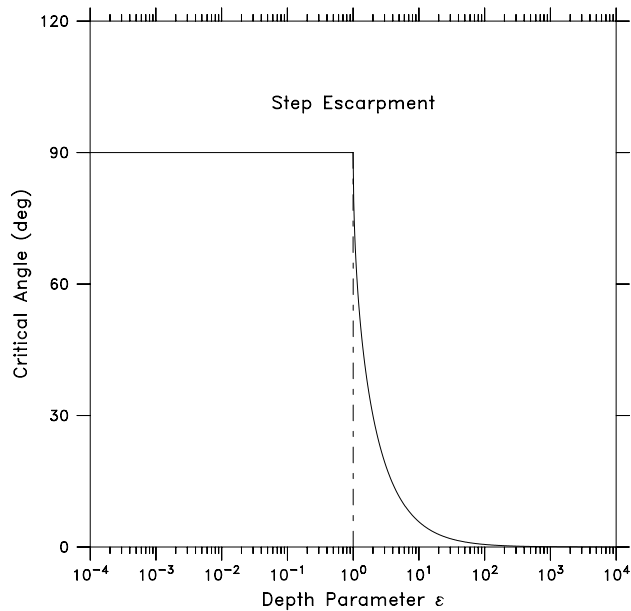
Figure 5: Critical angle ϕ_{crit} of incidence (above which waves are perfectly reflected) for a tsunami wave approaching a step escarpment from the shallow side, as a function of the depth parameter ϵ.

the condition on water transport is on its x-component

$$A_I + B_R = A_T \tag{47}$$

$$\cos\phi_0 \; [A_I - B_R] = \epsilon \cos\phi_1 \; A_T \;. \tag{48}$$

We define a modified form of the depth parameter as

$$\epsilon' = \epsilon \, \frac{cos\phi_1}{cos\phi_0} \tag{49}$$

where ϕ_1 is given be (43).

Dividing (48) by $\cos\phi_0$ and using (49), the matching conditions (47–48) then have the same form (39) as those for normal incidence, with ϵ' substituted for ϵ. The amplitude ratios for non-normal incidence can then be written down immediately

$$R'_T = \frac{2}{1+\epsilon'} \quad \text{and} \quad R'_R = \frac{1-\epsilon'}{1+\epsilon'} \qquad \text{for} \quad \epsilon < \epsilon_{crit} \tag{50}$$

and, noting that perfect reflection occurs for larger values of ϵ,

$$R'_T = 2 \qquad \text{and} \quad R'_R = 1 \qquad \text{for} \quad \epsilon \geq \epsilon_{crit} \;. \tag{51}$$

Figure 6 shows that R'_T and R'_R follow R_T and R_R closely when the incident wave approaches the escarpment from the deep-water side ($\epsilon \leq 1$). As ϵ increases, they continue to follow R_T and R_R until ϵ is near its cutoff
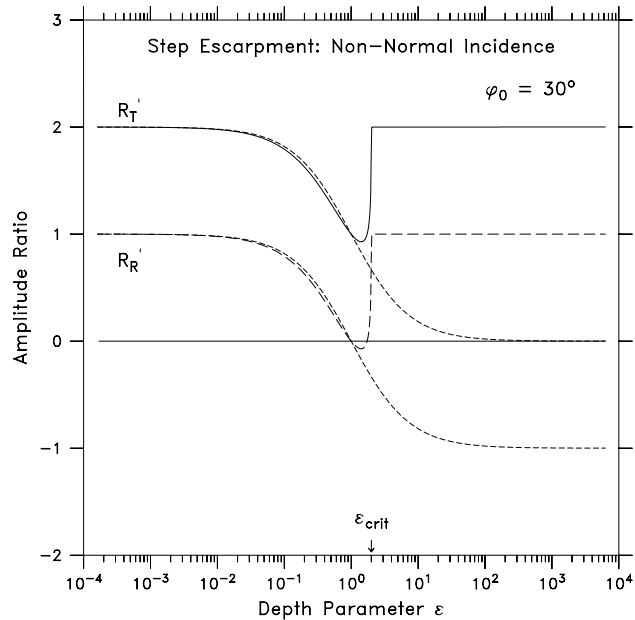
Figure 6: Amplitudes of reflected B_0 and transmitted A_1 tsunami waves resulting from the interaction of an obliquely incident wave with a step escarpment, as a function of the depth parameter $\epsilon = \sqrt{H_1/H_0}$. The amplitudes are shown as ratios relative to the amplitude A_0 of the incident wave, where the incident angle $\phi_0 = 30°$. $\epsilon > 1$ when the incident waves approach the escarpment from the shallow side.

ϵ_{crit}. In that neighborhood, both R'_T and R'_R increase rapidly toward the values (51) expected for perfect reflection. They remain at these values for $\epsilon > \epsilon_{crit}$. As seen in Figure 5, the depth parameter ϵ need not be much greater than unity before this condition of perfect reflection is reached.

3.3   Error Function Escarpment: Normal Incidence

In this subsection, we consider scattering off a low escarpment having an error function profile in the x-direction. The first order theory we will use is valid for topography in which only small changes in depth occur relative to the total depth. We assume normal incidence for the waves. When the depth profile across an escarpment has this profile, we can write the depth $H(x)$ as

$$H(x) = H_0 \left[1 + \frac{\epsilon^2 - 1}{\sigma\sqrt{\pi}} \int_{-\infty}^{x} e^{-\frac{x^2}{\sigma^2}} dx \right] . \tag{52}$$

As shown in Figure 7, H_0 is asymptotic depth ($x \to -\infty$) on the same side of the escarpment as the incident wave. If H_1 denotes the asymptotic depth ($x \to \infty$) on the other side of the escarpment, the depth parameter ϵ we will

Escarpment: Error Function Profile

Incident Wave η_0 $\rightarrow$

Reflected Wave ξ_0 $\leftarrow$ Transmitted Wave η_1 $\rightarrow$

H_1

H_0

x=0   x $\rightarrow$

Figure 7: Schematic diagram of an escarpment having an error-function shaped transition in depth between two constant-depth regions H_0 and H_1.

use is the asymptotic value

$$\epsilon \equiv \left[\frac{H_1}{H_0}\right]^{\frac{1}{2}} . \tag{53}$$

Since the fractional change in depth is small across the escarpment, it is convenient to define $\delta\epsilon$ as the deviation of ϵ from unity

$$\delta\epsilon \equiv \epsilon - 1 . \tag{54}$$

Here, $\delta\epsilon < 0$ when the incident wave approaches the escarpment from the deep-water side and $\delta\epsilon > 0$ when it approaches from the shallow side.

To discuss first-order scattering off this escarpment, it is convenient to focus on amplitude B_0 (35) of the back-scattered wave relative to the amplitude A_0 of the incident wave. For normal incidence ($\phi = 0°$) and to first order in $\delta\epsilon$, the scattering source term β (24) for an escarpment with an error function profile is

$$\beta \doteq \frac{\delta\epsilon}{2\sigma\sqrt{\pi}} e^{-\frac{x^2}{\sigma^2}} . \tag{55}$$

Then the modified amplitude B_0' (35) for the back-scattered wave is

$$B_0' \doteq -A_0' \frac{\delta\epsilon}{2\sigma\sqrt{\pi}} \int_{-\infty}^{\infty} \exp\left[2ik_0 - \frac{x^2}{\sigma^2}\right] dx \tag{56}$$

or

$$B_0 \doteq A_0 \frac{(-\delta\epsilon)}{2} e^{-k_0^2\sigma^2} . \tag{57}$$

Consistent with the step topography, this expression shows that the amplitude of the back-scattered wave (Figure 8) is independent of frequency when

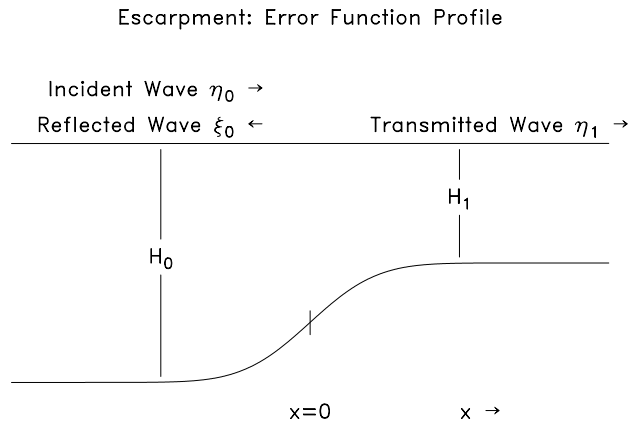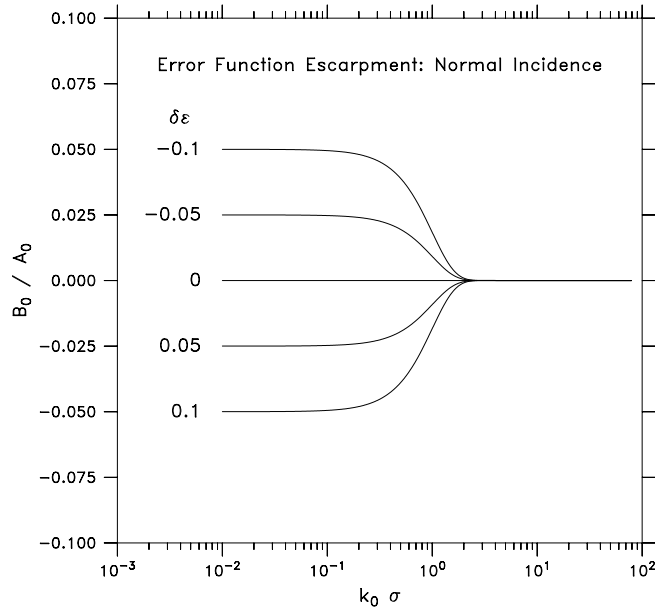**Figure 8**: Amplitudes B_0 of reflected tsunami waves resulting from the interaction of a normally incident wave ($\phi = 0°$) with a low error-function escarpment, as a function of the width-scale $k_0\sigma$, for various values of the deviation $\delta\epsilon$ of the depth parameter from constant depth ($\epsilon = 1$). The amplitudes are given as ratios relative to the amplitude A_0 of the incident wave.

the transition in depth across the escarpment occurs over a short distance compared with the tsunami wavelength

$$B_0 \doteq \frac{(-\delta\epsilon)}{2} A_0 \qquad \text{for} \quad k_0\sigma \ll 1 . \tag{58}$$

Conversely, the amplitude is negligible

$$B_0 \doteq 0 \qquad \text{when} \quad k_0\sigma > 2.5 . \tag{59}$$

In between, there is a range ($0.2 < k_0\sigma < 2$) in which the amplitude B_0 of the back-scattered wave changes rapidly with changes in the wavenumber k_0, and therefore changes in the wave frequency ω. Hence, there is a range of frequencies in which the scattering properties are dispersive (frequency dependent). This is even though it is often said tsunami waves are non-dispersive in the open ocean, in the shallow-water wave limit.

4.   Lineal Ridges and Trenches

This section considers lineal (straight) ridges and trenches surrounded by an abyssal plain of constant depth. Like the previous section on escarpments, it contains, first, an analysis of scattering off step topography (normal and non-normal incidence) and then an analysis for continuously varying topography

Rectangular Ridge
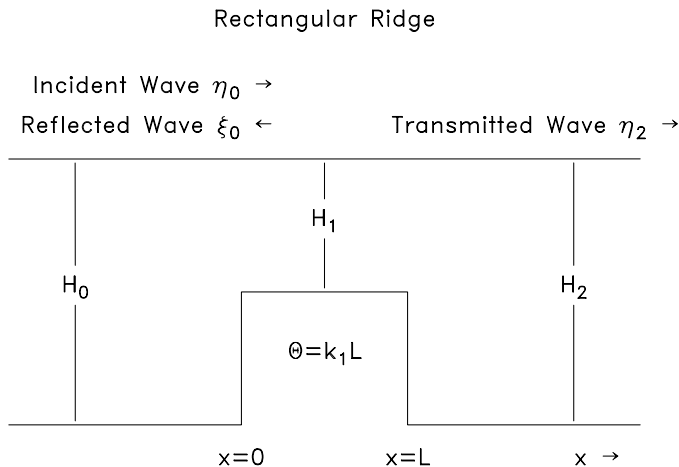

Figure 9: Schematic diagram of a rectangular ridge having a summit of constant depth H_1 and surrounded by a region of constant depth H_0. The sides of the ridge are vertical.

(Gaussian profile). The tsunami waves approach these features from the abyssal plain, rather than propagating as trapped waves along ridges. For a discussion of the latter, please see the recent paper by Koshimura *et al.* (1999).

The analysis for rectangular ridges leads the concept of minimum transmissivity, which leads in turn to a scattering index that can be used to assess the potential for finer-scale topography to scatter tsunami waves in the open ocean.

4.1 Rectangular Ridge: Normal Incidence

Figure 9 shows a tsunami wave (3) that is normally incident ($\phi = 0°$) on a rectangular ridge of width L and depth of H_1. The ridge is surrounded by an abyssal plain with the same depth ($H_0 = H_2$) on either side of the ridge.

The matching conditions (11 and 14) at the two depth transitions ($x_1 = 0$ and $x_2 = L$) can be written as conditions on the amplitudes (A_j, B_j). By assumption, $B_2 = 0$ since this is the amplitude of a wave that would be incident on the other side of the ridge. Four matching conditions then determine the remaining four amplitudes in terms of the amplitude A_0 of the incident wave.

We take the segment width δx_0 to be so small ($\delta x_0 \to 0$) that

$$\eta_0 = A_0 \quad \xi_0 = B_0 \qquad \text{at } x = x_1 \,. \tag{60}$$

Letting the phase shift across the ridge θ and the depth parameter $\epsilon \equiv \epsilon_1$ be defined by

$$\theta \equiv k_1 L \quad \text{and} \quad \epsilon \equiv \sqrt{\frac{H_1}{H_0}} \,, \tag{61}$$

the four matching conditions are then

$$A_0 + B_0 = A_1 + B_1 \tag{62}$$

$$A_0 - B_0 = \epsilon \left[A_1 - B_1 \right] \tag{63}$$

$$A_1 e^{i\theta} + B_1 e^{-i\theta} = A_2 \tag{64}$$

$$\epsilon \left[A_1 e^{i\theta} - B_1 e^{-i\theta} \right] = A_2 \, . \tag{65}$$

To solve (62–65) for the amplitudes in terms of the amplitude A_0 of the incident wave, it is convenient to first write B_0, A_1, and B_1 in terms of the amplitude A_2 of the transmitted wave and then write A_2 in terms of A_0

$$B_0 = -i \left(\frac{1 - \epsilon^2}{2\epsilon} \right) \sin \theta \, A_2 \tag{66}$$

$$A_1 = \left(\frac{1 + \epsilon}{2\epsilon} \right) e^{-i\theta} \, A_2 \tag{67}$$

$$B_1 = - \left(\frac{1 - \epsilon}{2\epsilon} \right) e^{i\theta} \, A_2 \tag{68}$$

where

$$A_2 = \left[\cos \theta - i \left(\frac{1 + \epsilon^2}{2\epsilon} \right) \sin \theta \right]^{-1} A_0 \, . \tag{69}$$

The amplitude B_0 (66) of the reflected wave is zero when either the ridge has the same depth as the surrounding region ($\epsilon = 1$) or the width of the ridge goes to zero ($\theta \to 0°$). For a given value of ϵ, B_0 is a maximum whenever the phase shift θ across the ridge is a multiple of 90°. Conversely, it is zero whenever $\theta = 0°, 180° \ldots$. These two extrema correspond to minimum transmission and perfect transmission of wave energy, respectively.

When ϵ is close to unity, the amplitude A_1 (67) is near A_2 and B_1 (68) is small, so that the incident wave is relatively unchanged as it propagates over the ridge. When the ridge is very shallow ($\epsilon \ll 1$), there is an apparent tendency for the on-ridge waves to have large amplitudes. However, we will see that the rectangular ridge produces artificial results in this parameter range, especially with regard to wave resonances on the ridge.

4.2   Rectangular Ridge: Transmissivity

Equation (69) leads to a formula for the magnitude of the ratio A_2/A_0 between the amplitudes of the transmitted and incident waves, which we will call the transmissivity

$$T = T_{min} \left[T_{min}^2 \cos^2 \theta + \sin^2 \theta \right]^{-\frac{1}{2}} \tag{70}$$

where the minimum transmissivity T_{min} is given by

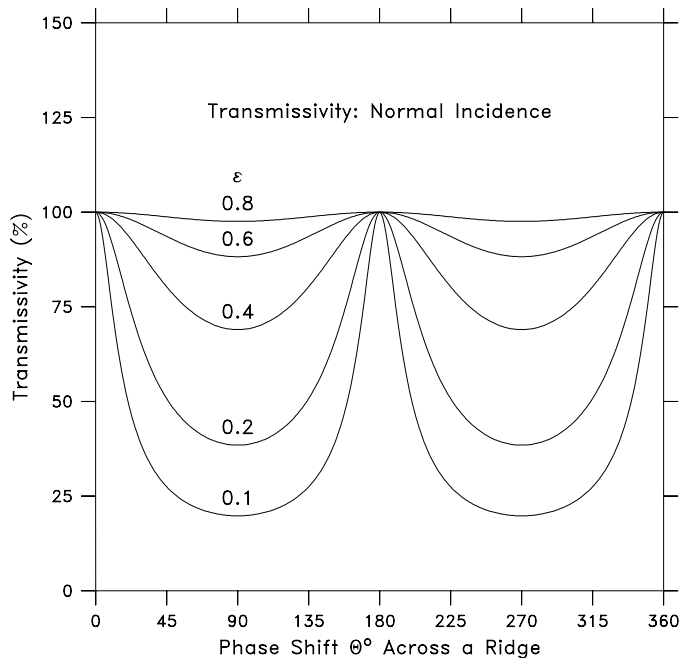$$T_{min} = \frac{2\epsilon}{1 + \epsilon^2} \, . \tag{71}$$

Figure 10: Transmissivity ($T = |A_2/A_0|$) for tsunami waves that are normally incident ($\phi = 0°$) on a rectangular ridge, as a function of the cross-ridge phase shift $\theta = k_1 L$ for various values of the depth parameter $\epsilon = \sqrt{H_1/H_0}$.

In the interpretation of the transmissivity given below, it is convenient to discuss it in terms of its percentage relative to perfect transmission (no topographic scattering by the ridge). Figure 10 shows that the transmissivity T (70) is a periodic function of the phase shift θ across the ridge. The maximum value ($T = 100\%$) occurs at $\theta = 0°$, $180°$ and integer multiples of the latter; while the minima ($T = T_{min}$) occur at $\theta = 90°$ and its odd multiples. When the ridge has low relief so that ϵ is close to unity, T remains close to 100%. This is regardless of the ridge width, as measured by the phase shift θ, and hence the wave frequency. The minimum value of T (Figure 10) decreases rapidly as ϵ increases over the range $\epsilon = 0.6 \to 0.2$, and the amount of scattering therefore tends to be a sensitive function of both ϵ and θ in this parameter range. At smaller values of ϵ (e.g., the $\epsilon = 0.1$ curve in Figure 10), the transmissivity is low over a broad range of the phase shift θ. To rise from low values to $T = 100\%$ at $\theta = 0°$, $180°$ and its multiples, the transmissivity T increases rapidly in the vicinity of these θ values. This increase is most pronounced when the depth parameter ϵ is small, corresponding to high ridges that reach close to the surface relative to the surrounding region.

The minimum transmissivity T_{min} (71) is a very useful measure of the potential that linear topographic features have to scatter tsunami waves in the open ocean. One distinct advantage of using it is that it depends only on the depth of the feature compared with the depth of the region immediately surrounding the feature. As seen in Figure 11, T_{min} forms a symmetric, bell-shaped curve when plotted versus $\log(\epsilon)$, with the peak of the curve at
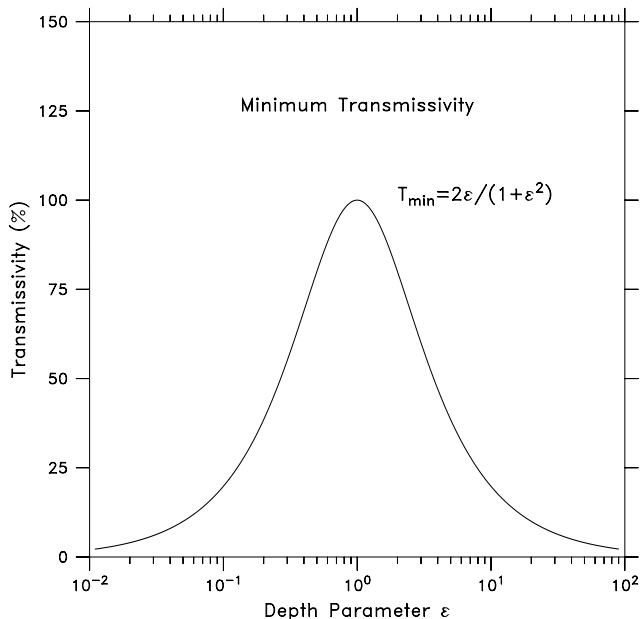
Figure 11: Minimum transmissivity T_{min} for tsunami waves that are normally incident ($\phi = 0°$) on a rectangular ridge, as a function of the depth parameter ϵ.

$\epsilon = 1$. Besides the behavior of T_{min} discussed in the previous paragraph, it is worth noting that near $\epsilon = 1$ the minimum transmissivity is a parabolic function of the deviation $\delta\epsilon \equiv \epsilon - 1$

$$T_{min} \doteq 1 - \frac{1}{2}\left(\delta\epsilon\right)^2 \ . \tag{72}$$

For rectangular trenches ($\epsilon > 1$), the minimum transmissivity T_{min} (Figure 11) decreases to small values as ϵ increases. However, the subsection 3.2 on escarpments shows that only a modest deviation from normal incidence is required to produce strong reflection, which corresponds to markedly decreased transmission. Further, even with normal incidence on a trench, increasing ϵ tends to decrease the phase shift across a trench and therefore diminishes the effect of the trench width on scattering. We must therefore regard scattering off trenches to be distinctly different in behavior from scattering off ridges, when ϵ deviates greatly from unity.

To understand how the transmissivity T varies with ϵ for fixed ridge width L and wave frequency ω, we note that the cross-ridge phase shift θ for normal incidence is given by

$$\theta = \frac{\theta_1}{\epsilon} \tag{73}$$

where θ_1 is the cross-ridge phase shift when $\epsilon = 1$. Because of their inverse relationship, θ increases as ϵ decreases and vice versa.

For $\theta_1 = 47°$, Figure 12 shows that as ϵ decreases from unity, the transmissivity T is closely approximated by the minimum transmissivity T_{min} for
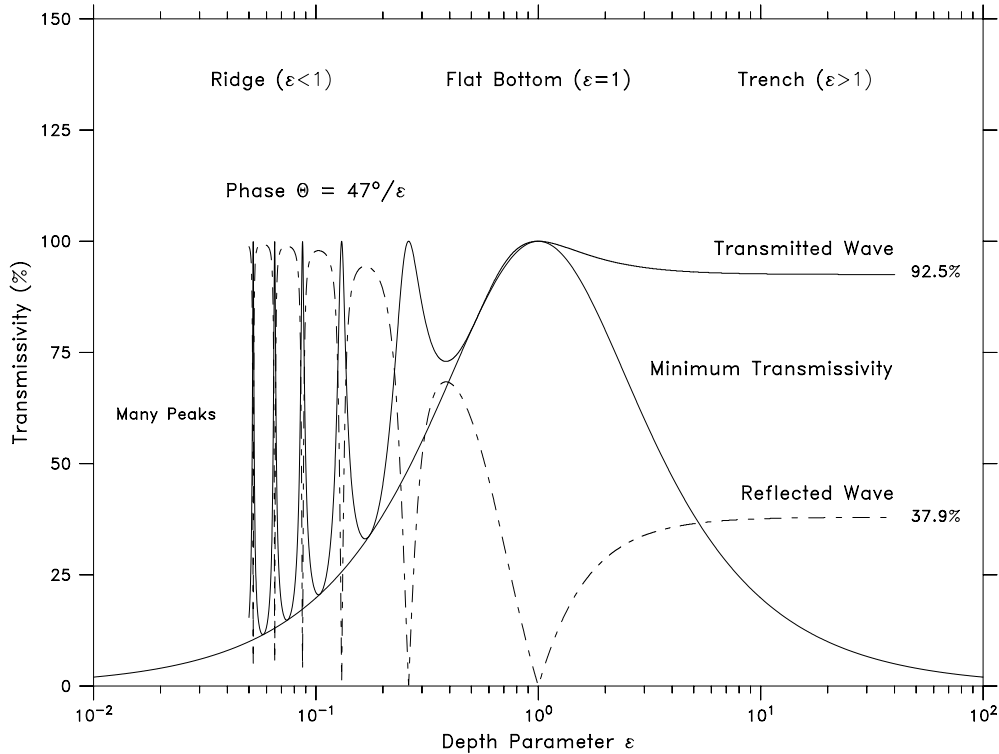
Figure 12: Transmissivity T for tsunami waves that are normally incident ($\phi = 0°$) on a rectangular ridge, as a function of the depth parameter ϵ for fixed frequency ω and ridge width L when the cross-ridge phase shift $\theta_{\epsilon=1} = 47°$.

a considerable range of ϵ. As ϵ decreases further, the phase shift θ (73) approaches 90°; the transmissivity then rises above T_{min} and reaches $T = 100\%$ when the ridge width is a quarter wavelength ($\theta = 90°$). The reflectivity ($R \equiv |B_0|/|A_0|$) is also plotted in Figure 12 to show the reciprocal relationship between T and R, in which $T^2 + R^2 = 1$.

As ϵ decreases further, T oscillates rapidly between T_{min} and 100% due to on-ridge resonances. Subsection 4.4 below will show that the higher-order resonances do not occur when the ridge has a Gaussian cross-section. Hence, whether they exist or not depends on the details of the cross-ridge depth profile; only the first case ($\theta = 90°$) is a robust feature of ridge scattering.

When $\epsilon > 1$, the behavior of T (Figure 12) is very different from the ridge regime. The T curve deviates almost immediately from T_{min} as ϵ increases from $\epsilon = 1$, decreasing smoothly toward a relatively high asymptotic value

$$T_{\epsilon \to \infty} \doteq \left[1 + \frac{1}{4} \, \theta_1^2 \right]^{-\frac{1}{2}} \tag{74}$$

where $\theta_1 < \frac{\pi}{2}$ is in radians. The transmissivity T (Figure 12) decreases monotonically toward $T_{\epsilon \to \infty}$ and there are therefore no passages of θ (73) through 90° as ϵ increases. For wide trenches, T may rise at least once to perfect transmission $T = 100\%$ before decreasing to $T_{\epsilon \to \infty}$. However, T still

has the general properties of deviating quickly from unity and remains much higher than T_{min} as ϵ increases further.

In conclusion, the analysis and examples given in this subsection show that when tsunami waves are normally incident on rectangular ridges, the transmissivity T (70) is closely approximated by T_{min} (71) over substantial ranges of the depth parameter ϵ and the width of the ridges, as measured by the cross-ridge phase shift θ. Hence, the minimum transmissivity T_{min} is a useful quantity for identifying those ridge-like features in the open ocean that are likely to cause significant scattering of tsunami waves and, conversely, the ones that allow the waves to pass without affecting the transmitted amplitude.

In contrast, T deviates quickly from T_{min} as ϵ increases over $\epsilon = 1$ and remains high, implying that rectangular trenches produce only weak scattering. This result is specific to normal incidence. The analysis of non-normal incidence on step escarpment (Section 3.2), in which the wave approaches obliquing from the shallow side (analogous to incidence on a wide trench), shows that there is a marked tendency for strong reflection and hence $T \ll 1$.

4.3   Rectangular Ridge: Oblique Incidence

The purpose of this subsection is to show that the transmissivities T (70) and T_{min} (71) are reasonable approximations for ridges over a substantial range of incident angles, even though they were derived for normal incidence.

We assume that the lineal ridge is still aligned with the y-coordinate. Then, letting ϕ_j be the angle in the jth segment that the wavenumber vector $\vec{k_j}$ makes with the x-axis, the x- and y-components of the wavenumber are

$$k_{x,j} = k_j \cos \phi_j \quad \text{and} \quad k_{y,j} = k_j \sin \phi_j, \tag{75}$$

where

$$k_j = \frac{\omega}{c_j} \,.$$

For a rectangular ridge, refraction decreases the incident angle ϕ_0 (Figure 13) to ϕ_1. Since $H_2 = H_0$, $\phi_2 = \phi_0$. The matching conditions then take the same form as (62–65) except that the depth parameter ϵ and the cross-ridge phase shift θ_1 are replaced by

$$\epsilon' = \epsilon \, \frac{\cos \phi_1}{\cos \phi_0} \tag{76}$$

and

$$\theta_1' = \theta_1 \sec \phi_1 \,. \tag{77}$$

Since the forms of the matching conditions are the same, it follows that the transmissivities for non-normal incidence have the same form as T (70) and T_{min} (71), when ϵ' and θ_1' are substituted for ϵ and θ_1

$$T' = T'_{min} \left[T'^{2}_{min} \cos^2 \theta_1' + \sin^2 \theta_1' \right]^{-\frac{1}{2}} \tag{78}$$

$$T'_{min} = \frac{2\epsilon'}{1 + \epsilon'^2} \,. \tag{79}$$
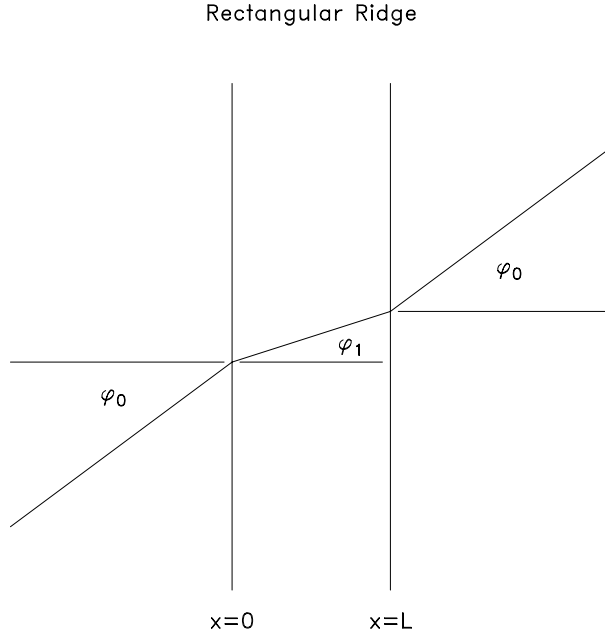
Rectangular Ridge

Figure 13: Schematic diagram showing the angles of incident ϕ_0, on-ridge ϕ_1, and transmitted $\phi_2 = \phi_0$ waves when an obliquely incident tsunami wave interacts with a rectangular ridge.

From Snell's law of refraction (derived from the condition $k_{y,0} = k_{y,1}$),

$$\phi_1 = \arcsin\left(\epsilon \sin\phi_0\right), \tag{80}$$

or

$$\phi_1 \simeq \epsilon\,\phi_0 \tag{81}$$
$$\text{for } |\epsilon| \lesssim 1 \text{ and } |\phi_0| \lesssim 30^\circ\,.$$

The decrease in the angle ϕ_1 over the ridge, as compared with the incident angle ϕ_0, acts to decrease the effect of oblique incidence on the transmissivities. We can see this explicitly by studying an approximate formula for T'_{min} as a function of ϵ_1 and ϕ_0. Noting that

$$\epsilon' \simeq \epsilon\,\frac{\cos\left(\epsilon\phi_0\right)}{\cos\left(\phi_0\right)} \tag{82}$$

$$\text{or} \quad \epsilon' \simeq \epsilon + \epsilon\left(1 - \epsilon^2\right)^2 \frac{\phi_0^2}{2}, \quad \phi_0 \text{ in radians,} \tag{83}$$

the minimum transmissivity T'_{min} is approximately (within 10%)

$$T'_{min} = T_{min} + \delta T'_{min}, \quad \delta T'_{min} \simeq \lambda\left(\epsilon\right)\phi_0^2 \tag{84}$$

where

$$\lambda\left(\epsilon\right) \equiv \epsilon\,\frac{\left(1 - \epsilon^2\right)^2}{\left(1 + \epsilon^2\right)^2}\,. \tag{85}$$
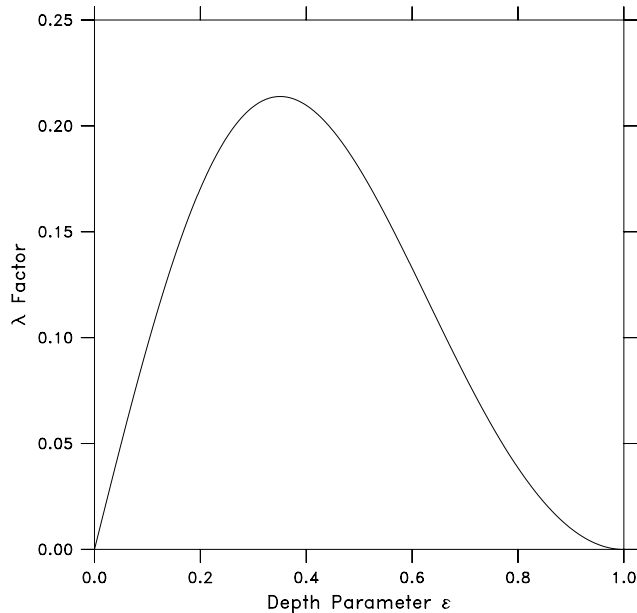
Figure 14: Transmissivity factor λ, as a function of the depth parameter ϵ.

As shown in Figure 14, the factor λ (85) is small over the full range of ϵ that is applicable to ridges ($0 \leq \epsilon < 1$). Its maximum value $\lambda_{\max} = 0.214$ occurs at $\epsilon = 0.351$.

The shapes of the deviations $\delta T'_{min}$ (Figure 15) follow that of $\lambda(\epsilon)$. However, they are scaled by an angular dependence ϕ_0^2 that reduces the deviation $\delta T'_{min}$ considerably (for $\phi_0 \leq 30°$). For instance, the maximum deviation $\delta T'_{min} = 0.059$ for $\phi_0 = 30°$. This corresponds to $<11\%$ of typical values for the normal-incidence T_{min}. Hence, the formula (71), derived for normal incidence ($\phi_0 = 0°$), is a reasonable approximation to the minimum transmissivity over a substantial range of incidence angles ϕ_0.

4.4   Gaussian Ridge: Normal Incidence

The first-order scattering theory for a low ridge having a Gaussian profile (Figure 16) provides a useful contrast to scattering off the rectangular ridge. The depth profile has the form

$$H(x) = H_0 \left[1 + (\epsilon^2 - 1) \, e^{-\frac{x^2}{\sigma^2}} \right] \tag{86}$$

where we define the depth parameter ϵ in terms of the minimum depth H_1 over the crest of the ridge and the depth H_0 of the surrounding region,

$$\epsilon \equiv \left[\frac{H_1}{H_0} \right]^{\frac{1}{2}} . \tag{87}$$
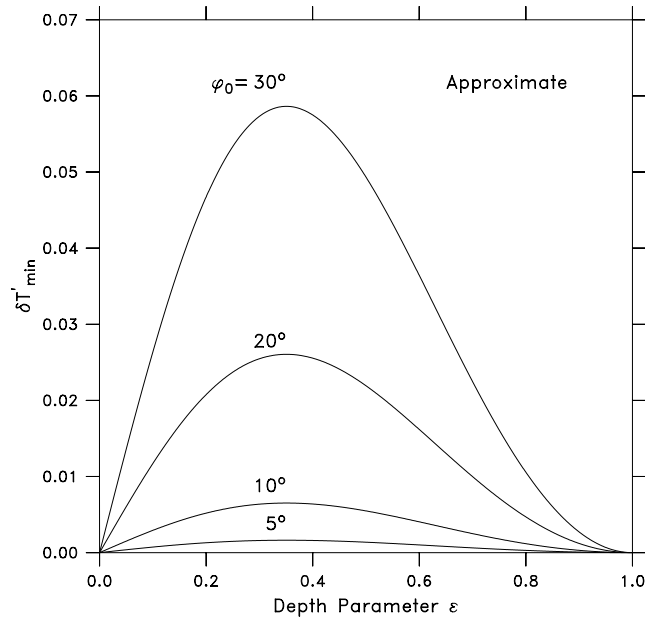
Figure 15: Deviation $\delta T'_{min}$ of the minimum transmissivity from unity, as a function of the depth parameter ϵ for various values of the incident angle ϕ_0.
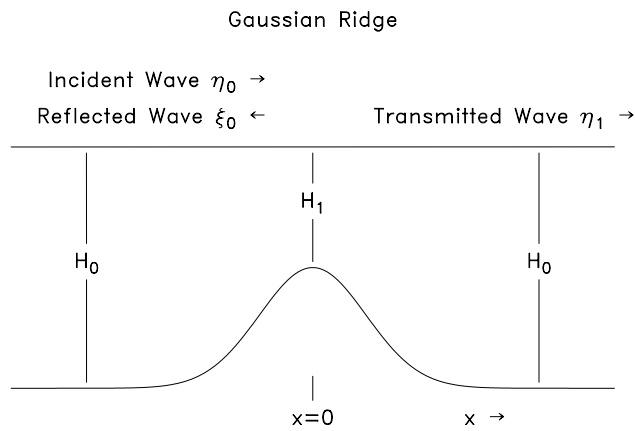

Figure 16: Schematic diagram of a ridge having a Gaussian cross-section with minimum depth H_1, surrounded by a region of constant depth H_0.

Following the same procedure (Section 3.3) that was used to develop scattering formulas for the error function escarpment, the β–factor for normal incidence ($\phi_0 = 0$) on a low Gaussian ridge is

$$\beta \doteq \frac{\delta\epsilon\, x}{\sigma^2}\, e^{-\frac{x^2}{\sigma^2}} \tag{88}$$

where $\delta\epsilon \equiv \epsilon - 1$.

Substituting this form into equation (35) leads to the integral relation for the amplitude B_0 of the reflected wave

$$B_0 \doteq -A_0\, \frac{\delta\epsilon}{\sigma^2} \int_{-\infty}^{\infty} x\, \exp\left[2ik_0 - \frac{x^2}{\sigma^2}\right] dx\,. \tag{89}$$

Integration by parts then leads to the explicit formula

$$B_0 \doteq iA_0\, (-\delta\epsilon)\, \sqrt{\pi}\, k_0\sigma\, e^{-k_0^2\sigma^2}\,. \tag{90}$$

The factor of $i = \sqrt{-1}$ in (90) causes the reflected wave to lag the incident wave in time by an additional 90°. This phase shift is due to the offset in space between the contributions that the up-slope and down-slope halves of the Gaussian ridge (Figure 16) make to the scattering process.

To illustrate how the amplitude of the reflected wave depends on the height of the Gaussian ridge and the wavelength, it is convenient to plot the ratio B_0 / iA_0, as a function of $k_0\sigma$ for various values of $\delta\epsilon$. As Figure 17 shows, the amplitude ratio is small for both low and high values of $k_0\sigma$, with a single maximum $(-\delta\epsilon)\sqrt{\pi/2e}$ that occurs between these regimes at $k_0\sigma = 1/\sqrt{2}$. The domain in which the ratio is a significant fraction of the maximum is roughly $0.05 < k_0\sigma < 2$. At low frequencies and therefore low wavenumbers, the ratio is proportional to $k_0\sigma$. At the high frequencies, the cutoff is exponentially sharp.

The interpretation of the low-frequency regime is that the up-slope and down-slope contributions to scattering nearly cancel. The net scattering that does occur is due to the slight offset of these slope areas relative to the wavelength. This spatial offset increases linearly with the product $k_0\sigma$. In the high-frequency regime ($k_0\sigma > 2$), the bottom slopes are too gentle to produce significant scattering. The wave behavior is then in the WKBJ regime.

To understand why the optimal scattering occurs at $k_0\sigma = 1/\sqrt{2}$, we note that the effective phase shift across the Gaussian ridge is about $\theta = 2k_0\sigma$. For the rectangular ridge, the lowest frequency resonance in scattering occurs when $\theta = 90°$, or $\theta = \pi / 2$ radians. Then, $k_0\sigma = 0.785$ which is within 12% of $1/\sqrt{2} = 0.707$. Hence, the optimal scattering for the Gaussian ridge occurs when the centers of the up-slope and down-slope regions are separated in distance by a quarter of a wavelength, which is the same condition that is needed for the lowest-frequency scattering resonance associated with the rectangular ridge.

Since the lowest-frequency scattering resonance is very similar for the Gaussian and rectangular ridges, this resonance appears to be a robust feature of the scattering process. Unlike the rectangular shape, however, the
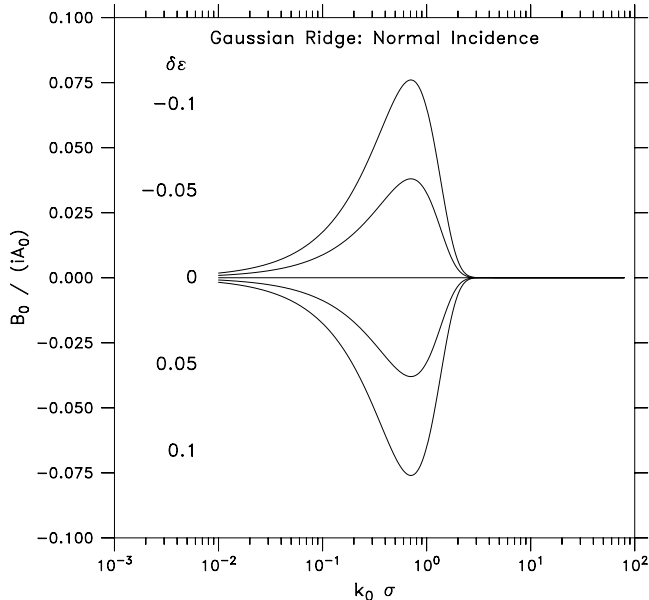
Figure 17: Amplitude B_0 of the reflected wave resulting from the interaction of a normally incident tsunami wave ($\phi_0 = 0°$) with a low Gaussian ridge, as a function of the ridge-width scale ($k_0\sigma$) for various values of the deviation $\delta\epsilon$ of the depth parameter $\epsilon = \sqrt{H_1/H_0}$ from unity. The amplitudes are shown as the ratio $B_0/(iA_0)$, where A_0 is the amplitude of the incident wave.

Gaussian shape does not lead to any higher-frequency resonances. Hence, the existence of the higher resonances depends on the detailed shapes of the topographic features.

The dependence (Figure 17) of the ratio B_0 / iA_0 on $\delta\epsilon$ is linear for low Gaussian ridges, in which the positive values of the ratio correspond to ridges ($\delta\epsilon < 0$) and negative values correspond to Gaussian trenches ($\delta\epsilon > 0$). As with low escarpments, an estimate of the amplitude of the transmitted wave can be made by invoking conservation of energy flux (6).

5. Circular Seamounts

This section revisits a standard topic in wave scattering theory, the scattering of plane waves off circularly symmetric seamounts and islands (e.g., Lamb, 1932; Meyer, 1995). The derivation generally follows those for lineal features, except that it is done in polar coordinates and involves sums of Bessel function solutions to the equations of motion.

Of particular interest are the conditions under which radially symmetric resonant scattering is likely to occur. This interest is prompted by model simulations showing concentric scattering features that occur when tsunami waves pass by the southern end of the Emperor Seamount Chain and the Mid-Pacific Mountains. The analysis is limited to seamounts hav-
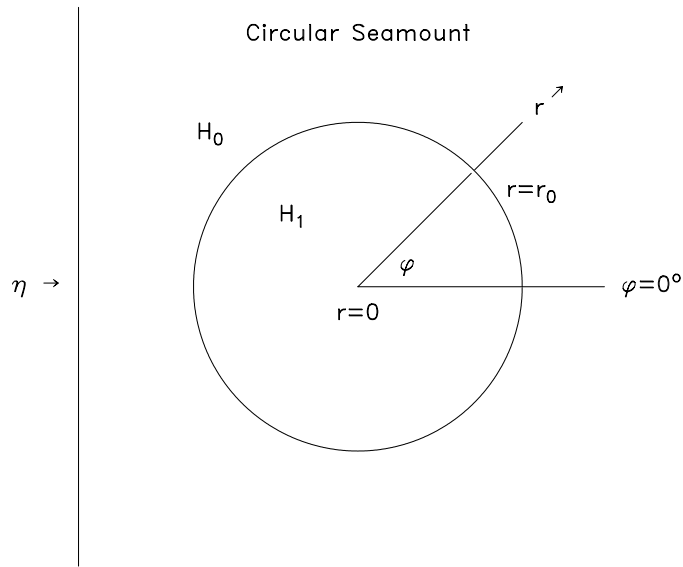
Figure 18: Schematic diagram of a circular seamount of radius r_0, having a summit of constant depth H_1 and surrounded by a region of constant depth H_0. The sides of the seamount are vertical.

ing constant-depth summits and vertical side-walls. For such seamounts, Meyer (1995) provides a detailed analysis of multiple resonances that are theoretically possible with this topography.

As shown in Figure 18, we use a polar coordinate system (r,ϕ) in which the origin is at the center of the seamount and the $\phi = 0°$ axis is in the direction that the incident wave is propagating. The seamount has a depth of H_1 and is surrounded by an abyssal plain having a constant depth H_0. The radius of the seamount is r_0. In terms of the incident wave η, the amplitudes of the scattered wave ξ and the wave ζ over the seamount are determined by matching the surface elevation and the radial components of water transport at the edge of the seamount $r = r_0$

$$\eta + \xi = \zeta \tag{91}$$

$$Q_r + R_r = S_r$$

or

$$c_0 \left[\frac{d\eta}{dr} + \frac{d\xi}{dr} \right] = c_1 \frac{d\zeta}{dr} \ . \tag{92}$$

Using the standard method of solution for 2-D scattering of plane waves off cylindrical objects, each wave is expanded into sums of products in which the angular dependences are cosine functions $\cos n\phi$. Letting n denote the

index of the sums

$$\eta = A_I \sum_{n=0}^{\infty} a_n J_n(k_0 r) \cos n\phi \tag{93}$$

$$\xi = A_I \sum_{n=0}^{\infty} h_n H_n^{(1)}(k_0 r) \cos n\phi \tag{94}$$

$$\zeta = A_I \sum_{n=0}^{\infty} b_n J_n(k_1 r) \cos n\phi \tag{95}$$

where J_n is the nth order Bessel function of the first kind and $H_n^{(1)}$ is the nth order Hankel function of the first kind, corresponding to outward propagation away from the seamount.

The coefficients a_n for a plane wave are

$$a_n = \begin{cases} 1 & \text{for} \quad n = 0 \\ 2\, i^{\,n} & \text{for} \quad n \geq 1 \end{cases}. \tag{96}$$

Since the angular functions $\cos n\phi$ are linearly independent, the matching conditions (91–92) reduce to equations in the coefficients

$$a_n J_n(\theta_0) + h_n H_n(\theta_0) = b_n J_n(\theta_1) \tag{97}$$
$$a_n J_n'(\theta_0) + h_n H_n'(\theta_0) = \epsilon\, b_n J_n'(\theta_1) \tag{98}$$

where $\theta_0 = k_0 r_0$ and $\theta_1 = \epsilon^{-1} \theta_0$. Here, the primes denote differentiation and it is understood that H_n is a Hankel function of the first kind.

Solving (97–98) for b_n and h_n

$$b_n = a_n \left[J_n'(\theta_0) H_n(\theta_0) - J_n(\theta_0) H_n'(\theta_0) \right] / D \tag{99}$$

$$h_n = a_n \left[J_n'(\theta_0) J_n(\theta_1) - \epsilon\, J_n(\theta_0) J_n'(\theta_1) \right] / D \tag{100}$$

where

$$D \equiv \epsilon\, J_n'(\theta_1) H_n(\theta_0) - J_n(\theta_1) H_n'(\theta_0) \,. \tag{101}$$

The angular dependence and intensity of scattering that occurs as a function of the depth parameter ϵ can be seen by plotting the ratio $|h_n|/|a_n|$. Figure 19 shows that over a considerable range ($\epsilon > 0.15$), dipole scattering ($n = 1$) is most important. The intensity of scattering in this regime is small ($|h_n|/|a_n| < 0.08$).

In contrast (Figure 19), the intensity of the monopole scattering (n=0) increases rapidly as ϵ decreases and dominates the scattering process around the values of ϵ and $\theta_0 = k_0 r_0$ corresponding to the lowest-frequency resonance over the seamount, where $J_0(\theta_1) \doteq 0$. This, and other resonances, can also be seen in the plots (Figure 20) of on-seamount b_n magnitudes. As with the rectangular ridge, the presence (or absence) of higher resonances is likely to depend very critically on the details of the topography. However, the lowest

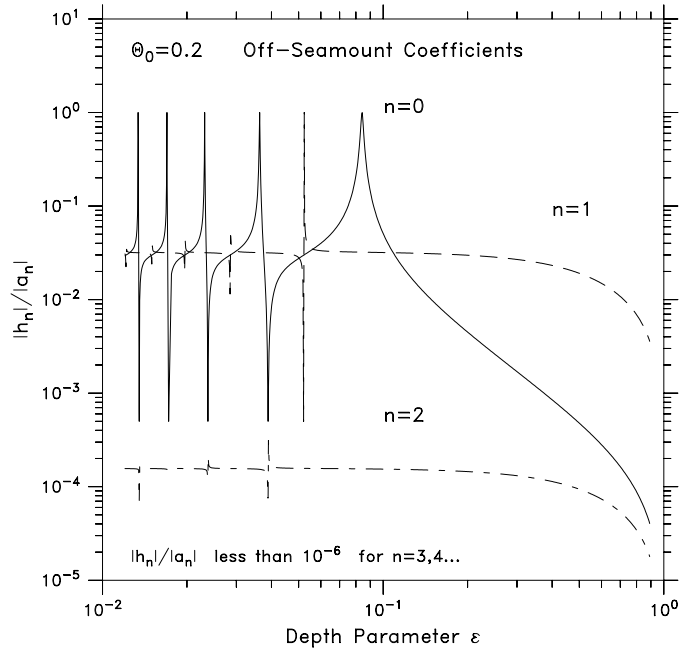**Figure 19**: Magnitudes of the off-seamount coefficients h_n for scattered wave components, as a function of the depth parameter $\epsilon = \sqrt{H_1/H_0}$ for the non-dimensional radius $\theta_0 = 0.2$. The magnitudes are shown as ratios relative to corresponding coefficient a_n for the incident plane wave.
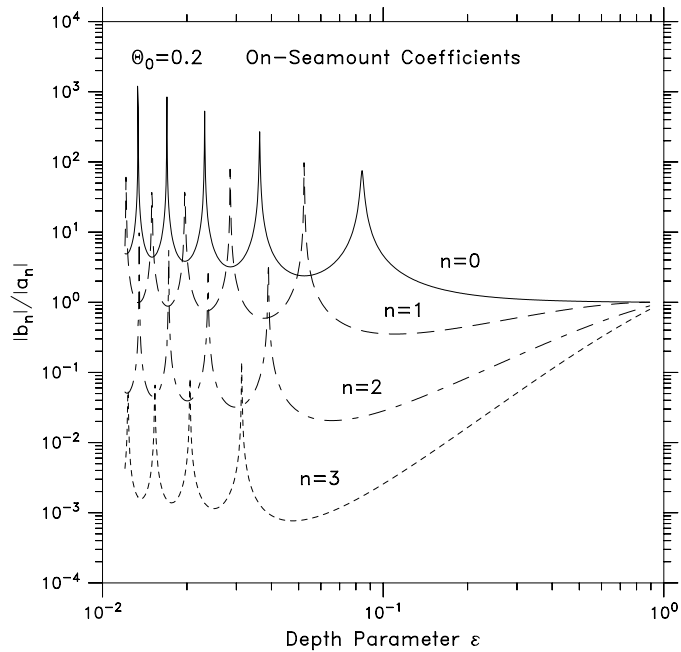

Figure 20: Same as Figure 19 but for the on-seamount coefficients b_n.

resonance is likely to be a robust feature that is insensitive to the details of the topography.

From the analysis of scattering from circular seamounts with constant-depth summits and vertical side-walls, we see that the scattering tends to be weak and dominated by dipole ($n = 1$) scattering. The exception is when the wave frequency, seamount radius, and relative depth allow a monopole ($n = 0$) resonance to occur over the seamount. In this case a strong, radially symmetric pattern will be seen radiating from the seamount as a tsunami wave passes.

6.   Discussion

In this section, we use the analytic theory to address several important issues concerning tsunami wave scattering in the North Pacific. The first issue is how shallow must a topographic feature be to scatter significant tsunami energy and, further, how shallow must it be before it will almost certainly interact strongly with tsunami waves. Since the minimum transmissivity T_{min} (71) is large when the interaction of tsunami waves with topography is small and small when the interaction is large, it is useful to define a scattering index

$$S \; = \; 1 \; - \; T_{min} \; . \tag{102}$$

This index has the convenient property that it is small when the scattering is small, and large when it is large. Since T_{min} is bounded between zero and unity, so is S. Based on the theory presented in this memorandum, this index provides an effective tool for identifying those topographic features in the ocean that are likely to scatter or reflect significant tsunami wave energy.

As shown in Figure 21 and Table 1, a feature needs to be shallower than 3000 m in order to produce even a small amount of scattering ($S \geq 0.01$) for the regional depths ($H_0 = 4000$–6000 m) that occur in the open North Pacific. It needs to be <1500 m to produce substantial scattering ($S \geq 0.2$) and will almost certainly have a major effect on tsunami waves ($S \geq 0.5$) if it is shallower than 400 m.

Hence, tsunami wave scattering between the Alaska-Aleutian Subduction Zone and Hawaii (Figure 22) is small because of the large depths of topographic features in this region. Titov *et al.* (1999) verify this result by show-

Table 1: Feature depth H_1 (m), as a function of depth H_0 (m) of the surrounding region and the scattering index S.

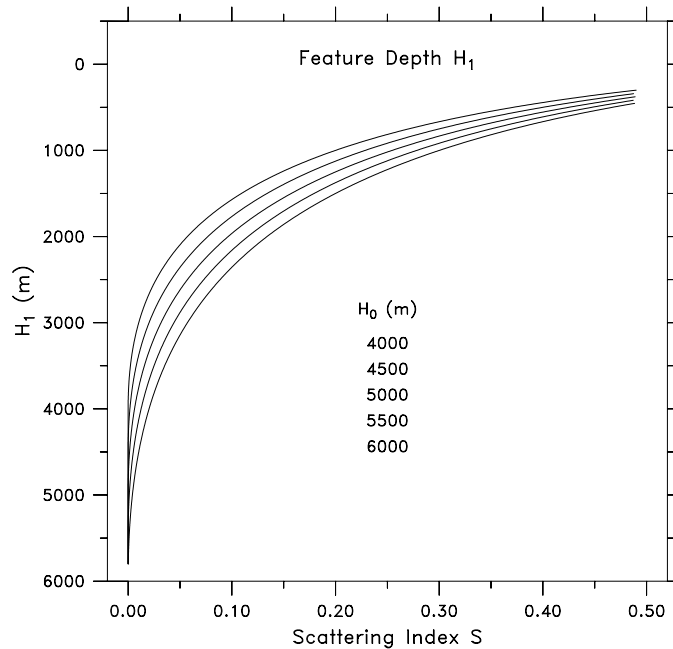| H_0 S :	0.01	0.05	0.10	0.20	0.50
4000	3011	2096	1571	1000	287
4500	3387	2358	1768	1125	323
5000	3764	2620	1964	1250	359
5500	4140	2883	2161	1375	395
6000	4516	3145	2357	1500	431

Figure 21: Depth H_1 of topography features as a function of the scattering index S, for different values of the depth H_0 of the surrounding region. Based on normally incident tsunami waves interacting with rectangular ridges.

ing that tsunamis propagating southward from the AASZ are sensitive only to the regional variations in topography. This is based on a one-dimensional numerical model (single-frequency tsunamis propagating southward along 157°W) and MOST model simulations for tsunamis generated in the AASZ.

There are, however, high features farther west and south that interact strongly with tsunami waves. These are the Emperor Seamount Chain, the Hess and Shatsky Rises, the Mid–Pacific Mountains, the Musician Seamounts, and the Hawaiian Ridges themselves. In addition, the Aleutian–Komandorskiye and Kuril Island Arcs are major barriers to tsunamis. There are also likely to be significant topographic interactions in the continental margin off the U.S. West Coast, British Columbia, and Southeastern Alaska, due to the complex topography associated with the Alaskan Seamounts, the Endeavour and Juan de Fuca Ridges, the Gorda Fracture Zone, and the Mendocino Escarpment.

The geographic extent of a topographic feature is also important in terms of how strongly it interacts with tsunami waves. A useful measure of this extent is the width of a feature corresponding to its lowest frequency resonance. These resonances are the most likely to occur and the least sensitive to the details of the topography. Also, many ridges and large seamounts have flat tops due to erosion that occurred when these features extended very close to the sea surface.

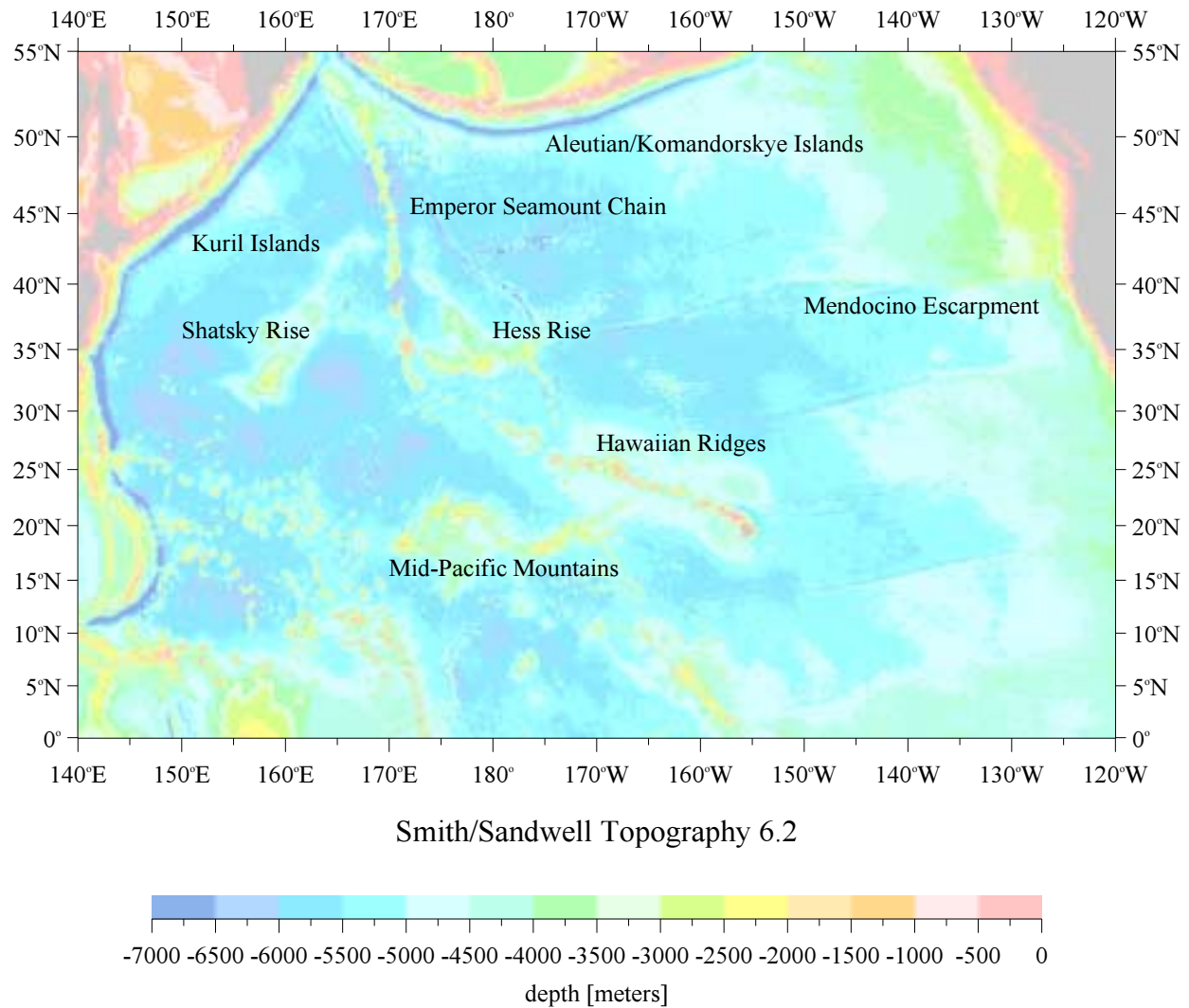Smith/Sandwell Topography 6.2

Figure 22: Smith-Sandwell topography for the North Pacific Ocean. Features in the open ocean with depths <1500 m are likely to scatter a significant amount of tsunami wave energy, while features with depths <400 m are likely to have a major impact on passing tsunami waves.

6.1 Ridges and Seamounts

For tsunami waves that have normal incidence $\phi = 0°$ on rectangular ridges (Section 4.1), this resonance occurs when the cross-ridge width is a quarter-wavelength $(k_1 L_{\frac{1}{4}} = 90°)$ as computed from the wave period τ and the ridge depth H_1

$$L_{\frac{1}{4}} = \frac{\tau}{4} \sqrt{gH_1} \tag{103}$$

For circular seamounts having flat tops, the corresponding resonance occurs very near the first zero of the zero-order Bessel function $[J_0(k_1 r_0) = 2.405]$. The diameter of the seamount at this resonance is then

$$D_0 = \frac{2.405}{\pi} \tau \sqrt{g H_1} \tag{104}$$

Over the range of tsunami wave periods $\tau = 5–50$ min, there is a wide range of the possible widths and diameters (Table 2) that allow the lowest frequency resonances to occur. However, the most tsunami energy will be scattered by the shallower ($H_1 \leq 400$ m) seamounts. In this case, the horizontal scales range from <10 km to 160 km. Here, the shorter scales correspond to short-period tsunamis incident on shallow features, and the longer scales to long-period tsunamis incident on deep features. The signatures of these resonances in observed tsunamis and numerical simulations are strong reflections by ridges and strong circular patterns eminating from seamounts.

Further application of the theory to ridges and seamounts in the North Pacific is made difficult by the complex nature of these features. For instance, the Emperor Seamount Chain (Figure 22) has numerous short ridge segments that are topped by seamounts and separated by deep passes. Such irregular topography over a wide range of scales is also seen along the Aleutian/Komandorskiye and Kuril Island Arcs and the Hawaiian Ridges. The other major features (Hess and Shatsky Rises, Mid-Pacific Mountains, Musician Seamounts and the eastern continental margin off the U.S. West Coast, British Columbia, and Southeastern Alaska) has complicated topography as well.

6.2 Escarpments and Trenches

Escarpments can cause strong reflections when the tsunami waves approach these features obliquely from the shallow side. This is provided the depth contrasts are large enough across the escarpments. Given the criteria developed in Section 3, the only escarpment in the North Pacific (Figure 22) that has a large enough depth contrast to strongly reflect tsunami waves is the eastern segment of the Mendocino Escarpment, near the U.S. West Coast. The effect of the escarpment is enhanced by a ridge that runs westward along its crest from the coast to 129°W. These tsunami waves need to approach from the northern side at non-normal incidence. Hence, there is a tendency for tsunamis generated in the AASZ and Kamchatka regions to be partially reflected toward the north when they reach the easternmost

Table 2: Ridge width (103) and seamount diameter (104) corresponding to the lowest frequency resonances, as functions of tsunami wave period and depth of the feature. The diameters are 3.06 times the widths, for the same period and depth.

Period (min)	Depth (m)	Ridge Width (km)	Seamount Diameter (km)	Period (min)	Depth (m)	Ridge Width (km)	Seamount Diameter (km)
5	100	2	7	30	100	14	43
	500	5	16		500	32	96
	1000	7	23		1000	45	136
	1500	9	28		1500	55	167
10	100	5	14	40	100	19	58
	500	11	32		500	42	129
	1000	15	46		1000	59	182
	1500	18	56		1500	73	223
20	100	9	29	50	100	23	72
	500	21	64		500	53	161
	1000	30	91		1000	74	227
	1500	36	111		1500	91	278

segment of the Mendocino Escarpment. It will also produce some reflection of tsunami waves generated in the Cascadia Subduction Zone, which lies immediately north of the escarpment.

While the North Pacific (Figure 22) is bounded along its northern and western margins by deep trenches, the theory presented in Section 4 indicates that these features produce very little scattering for a relatively wide range of incident angles. However, they do contribute to wave trapping of tsunamis on the adjacent continental shelves and tsunami propagation along the shelves and continental slopes. They do this by decreasing the incident angle necessary for trapping (evanescent off-shelf wave). The Emperor and Chinook Trenches, located east of the Emperor Seamount Chain, do not scatter significant tsunami wave energy because the surrounding region is so deep.

6.3   Transient Tsunamis

Real tsunamis are transient events that can be thought of as the sum of single-frequency components, where the dominant components of a real tsunami tend to occur within a relatively narrow frequency band. Hence, the general results of the single-band theory can be applied to these tsunamis.

Scattering and reflections extend the duration of real tsunamis in the North Pacific. Since these processes depend on the wavelength of the tsunamis relative to the horizontal scales of the topography, this topography also causes dispersion in the tsunami waves. This is even when they satisfy the long-wave equations, which are non-dispersive for constant depth. They also contribute to the random appearance of tsunami time series observed at tide gages as various decaying wave components interfere with each other (Mofjeld *et al.*, 1999a).

The theory has focused on tsunami wave scattering from isolated topographic features. However, the pattern from even a small number of scatterers located near each other is very difficult to interpret. Numerical models (e.g., Mofjeld *et al.*, 1999b; Titov *et al.*, 1999) are then the appropriate tools to study the combined effects of realistic topography. Numerical simulations also go beyond a frequency analysis to an analysis of tsunami wave scattering when these waves have realistic tsunami patterns in time. The analytic theory provides essential tools for interpreting the model simulations.

7.   Conclusions

Based on the analytic theory presented in Sections 3–7, we are led to the conclusions shown in Table 3.

The theory also leads to quantities, based on the water depth, that can be used to assess whether topographic features are likely to cause significant scattering and/or wave reflection. Of particular value is the scattering index S. The application of this index to the North Pacific Ocean is given in the Discussion Section.

Numerical tsunami models of the North Pacific that do not resolve these features adequately, either by lacking spatial resolution or using smoothed topography, will not properly simulate the interaction between these features and tsunamis. The theory presented in this memorandum provides simple, yet powerful, tools for interpreting these interactions.

8.   Acknowledgments

Table 3: Conclusions

Feature Type	Depth Profile	Incident Angle	Conclusions
Basic Formulation (lineal features)	Step	Normal	Scattering and reflection depend on the depth of a feature, relative to the depth of the surrounding region, and on wave frequency.
		Oblique	Wave direction becomes more normal when the feature is shallower than its surroundings and more oblique when propagating into deeper water (sometimes reflecting the waves).
	Continuous	Normal	Local scattering strength is proportional to the logarithmic gradient of the depth. Otherwise, wave amplitudes are controlled by Green's $\frac{1}{4}$th–law and phases by the spatial integral of the local phase gradient.
Escarpments	Step	Normal	Reflection off an abrupt escarpment is independent of wave frequency and is strongest at large depth contrasts.
		Oblique	Perfect reflection can occur as waves attempt to propagate into deeper water (when incident angle is large enough).
	Error Function	Normal	Narrow-width escarpments behave like the step escarpment; the behavior is a sensitive function of frequency when the product of wavelength times width scale is order unity; gently sloping features produce negligible scattering.
Ridges	Rectangular	Normal	The scattering index, based on minimum transmissivity, is a useful tool for identifying important scattering features. Strongest reflections (lowest transmission) occur when the cross-ridge phase shift is an odd multiple of $90°$, and weakest for a multiple of $180°$. Narrow ridges produce only weak reflections, unless they are very high.
		Oblique	Refraction causes behavior to be much like the normal-incidence case, over a substantial range of incident angles. (Ridge-trapped waves are not considered in the theory.)
	Gaussian	Normal	The minimum transmission matches closely the first minimum for the rectangular ridge, but the other (higher frequency) minima are missing; hence the first minimum is a robust feature of ridge topography, but the others are not. Smooth, broad ridges produce only weak reflections (high transmissivity).
Trenches	Rectangular	Normal	Trenches produce little reflection at normal incidence, even when they are deep.
		Oblique	Trenches can enhance shelf/slope trapping of tsunami waves near subduction zones.
Circular	Flat-Top	(Plane waves)	The scattering by seamounts is weak and forms a dipole pattern, except for the lowest-frequency monopole (radially symmetric) resonance. In this case, the amplitude on the seamount is substantially larger than the amplitude in the surrounding region.

9.   References

Carrier, G.F. (1971): The dynamics of tsunamis. In *Mathematical Problems in the Geophysical Sciences*, W.H. Reid, (ed.), American Mathematical Society, 157–187.

González, F.I., E.N. Bernard, H.B. Milburn, V.V. Titov, H.O. Mofjeld, M.C. Eble, J.C. Newman, R.A. Kamphaus, and C.L. Hadden (1999): An integrated approach to improving tsunami warning and mitigation. *Oceans '99 MTS/IEEE Abstracts.*

Koshimura, S., F. Imamura, and N. Shuto (1999): Propagation of obliquely incident tsunamis on a slope Part II: characteristics of on-ridge tsunamis. *Coast. Eng. J.*, 41(2), 165–182.

Lamb, H. (1932): *Hydrodynamics.* Dover, 738 pp.

Meyer, R.E. (1995): On the interaction of water waves with islands. In *Long-Wave Runup Models*, H. Yeh, P. Liu and C. Synolakis (eds.), World Scientific, 3–24.

Mofjeld, H.O., F.I. González, and J.C. Newman (1999a): Tsunami prediction in U.S. coastal regions. *Coastal Ocean Prediction*, C.N.K. Mooers (ed.), American Geophysical Union, 353–375.

Mofjeld, H.O., V.V. Titov, F.I. González, and J.C. Newman (1999b): Tsunami wave scattering in the North Pacific. *IUGG 99 Abstracts, Week B*, July 26–30, 1999, B.132.

Titov, V.V., H.O. Mofjeld, F.I. González, and J.C. Newman (1999): Offshore forecasting of Alaska-Aleutian Subduction Zone tsunamis in Hawaii. NOAA Tech. Memo. ERL PMEL-114, PMEL, Seattle, WA, 22 pp.